Ballistic transport of a polariton ring condensate with spin precession

Q. Yao [1] E. Sedov,[2,3,4,5] S. Mukherjee,[6] J. Beaumariage,[1] B. Ozden,[7] K. West,[8] L. Pfeiffer,[8]
A. Kavokin,[2,3,4,5,9] and D. W. Snoke[1]

[1]*Department of Physics and Astronomy, University of Pittsburgh, 3941 O'Hara Street, Pittsburgh, Pennsylvania 15260, USA*
[2]*Key Laboratory for Quantum Materials of Zhejiang Province, School of Science, Westlake University,
18 Shilongshan Road, Hangzhou 310024, Zhejiang, China*
[3]*Westlake Institute for Advanced Study, 18 Shilongshan Road, Hangzhou 310024, Zhejiang, China*
[4]*Spin Optics Laboratory, Saint Petersburg State University, Ulyanovskaya 1, Saint Petersburg 198504, Russia*
[5]*Russian Quantum Center, 100 Novaya Street, Skolkovo, Moscow Region, 143025, Russia*
[6]*Joint Quantum Institute, University of Maryland and National Institute of Standards and Technology,
College Park, Maryland 20742, USA*
[7]*Department of Physics, Penn State Abington, Abington, Pennsylvania 19001, USA*
[8]*Department of Electrical Engineering, Princeton University, Princeton, New Jersey 08544, USA*
[9]*Moscow Institute of Physics and Technology, Dolgoprudnyi, Moscow Region 141701, Russia*

It is now routine to make Bose-Einstein condensates of polaritons with long enough lifetime and low enough disorder to travel ballistically for hundreds of microns in quasi-one-dimensional (1D) wires. We present observations of a nonequilibrium polariton condensate injected at one point in a quasi-1D ring, with a well-defined initial velocity and direction. A clear precession of the circular polarization is seen, which arises from an effective spin-orbit-coupling term in the Hamiltonian. Our theoretical model accurately predicts the experimentally observed behavior and shows that "zitterbewegung" behavior plays a role in the motion of the polaritons.

Ring condensates have been studied in several systems (e.g., Refs. [1–4]), including in exciton-polariton condensates [5], where it has been shown that quantum phase coherence around the ring has led to quantized circulation analogous to quantized vortices in liquid helium. Several other experiments [6–10] have also studied polariton condensates in a ring geometry, but have primarily shown spatial pattern formation due to an incoherent mechanism, namely an instability in the interaction between the condensate and a thermal reservoir, leading to a natural length scale for self-trapping [11].

In the present work, we report direct imaging of a polariton condensate as it moves ballistically and coherently in a circular ring. In these experiments, the initial velocity and direction of the condensate is determined by the position of the point of injection of the condensate into the ring. Although the condensate is in a single energy state, its polarization precesses around the ring, because of a term in the Hamiltonian analogous to the spin-orbit coupling which also gives "zitterbewegung" [12–17], that is, side-to-side motion of a ballistic wave packet. Because the polaritons have extremely light mass, of the order of $10^{-4} m_0$, where m_0 is the free-space mass of an electron, they have long wavelength at easily obtainable temperatures, which makes the ballistic paths large enough (tens of microns) to see by standard optical imaging.

I. EXPERIMENTAL METHODS

The microcavity sample was grown on a GaAs (001) substrate by molecular beam epitaxy. It consists of a $3\lambda/2$ microcavity and three sets of four GaAs quantum wells placed at the antinodes of the cavity photon mode. Two AlGaAs/AlAs distributed Bragg reflectors (DBRs) were used to create the microcavity, with 32 periods in the top DBR and 40 periods in the bottom DBR. Individual pieces measuring 5 mm × 5 mm from the center of the wafer were used to construct the ring structures. It is worth noting that the wafer's centers are flatter than the remainder, allowing for consistent photon energy across the ring structures. The detuning of the ring is −12.38 meV, corresponding to 76% photonic fraction. The Rabi splitting is ∼19.6 meV according to the characterization results before the sample was etched. The array of ring structures with a radial width of approximately 15 μm and a diameter of 100 μm was fabricated using standard photolithography techniques. The top DBR was dry-etched to ring shape with a 20:7 BCl_3/Cl_2 inductively coupled plasma (ICP) reactive ion etch at 3.0-mT chamber pressure, 600-W ICP power, and 75-W RF bias power.

During the experiment, a continuous-wave Ti:sapphire laser, actively locked at $E_{pump} = 1705.6$ meV ($\lambda = 727$ nm), was used to nonresonantly pump the sample through a 20 × 0.4-N.A. microscope objective. A mechanical chopper with a 1.7% duty cycle at 400 Hz was placed in the laser path to reduce heating. All reported powers are the peak power of each short pulse. The pump spot was ≈8 μm full width at half maximum. The same microscope objective was used to capture photoluminescence (PL) from the ring of 1593 meV (778 nm). The reflected laser was blocked by an energy filter (750-nm
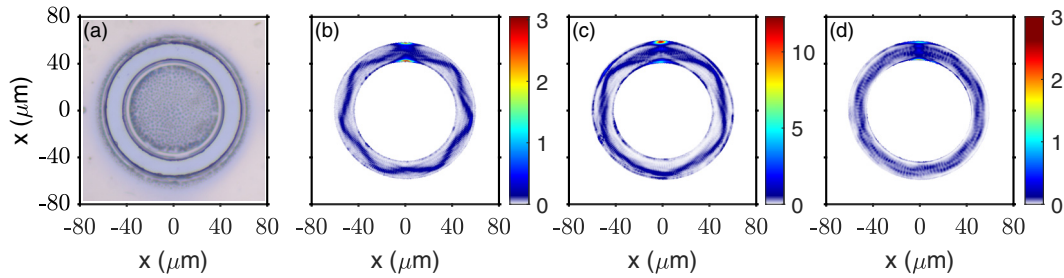
FIG. 1. (a) Optical image of the typical ring structure. (b)–(d) A series of intensity-normalized real-space images of the light emission from polariton condensate in a ring trap, with slightly different pump positions (the pump is moved in the radial direction). The pump power was about $6P_{th}$, where P_{th} was the critical threshold for Bose condensation.

long-pass filter). Both real-space images and energy-resolved images were taken with a charged-coupled device camera. We also obtained angle-resolved imaging by switching the lens combination. Half-wave plates, quarter-wave plates, and polarizers were utilized for polarization measurement, which is similar to that in Ref. [18]. All measurements were performed by cooling the microcavity to low temperature (below 10 K) in a continuous-flow cold-finger cryostat. Details of the experimental setup can be found in the Supplemental Material [19]. The images were normalized by camera integration time, image counts, and the power of the neutral density filter in front of the camera. The normalized image looks the same as the raw data with proper color scales.

II. EXPERIMENTAL APPROACH AND RESULTS

Exciton-polaritons in a microcavity, called here simply polaritons, are mixed states of excitons and photons, which have the property of repulsive interactions due to their excitonic component, while having very light mass due to their photonic component. Numerous experiments have shown the effect of Bose-Einstein condensation of polaritons (e.g., Refs. [20,21]; for a review see Ref. [22].) The polariton condensate is typically created at bath temperatures of 4 K; in our experiment, the condensate is out of equilibrium but still has long-range phase coherence, although under proper conditions of confinement it can reach equilibrium [23].

For these experiments we used an AlGaAs/GaAs microcavity structure with very high Q (ca. 300 000), very similar to the structures used in prior experiments [24,25] which showed ballistic motion of polaritons over hundreds of microns. These microcavities were etched into ring structures with a radial width of approximately 15 μm and a diameter of 100 μm. Figure 1(a) shows a typical structure. In prior experiments with polaritons in rings like these [18,26], there was a gradient of potential energy of the polaritons across the rings, which caused the polaritons to eventually settle into the lowest-energy point on one side of the ring. In the present experiments, great care was taken to have a very flat potential-energy profile around the rings, so that the polaritons flow freely around the ring without attraction to any one location.

Residual strain from the etching process creates a strain profile in the rings in the radial direction that leads to a potential-energy barrier that deters the polaritons from leaking out the sides. Therefore, the polaritons are confined to

a quasi-one-dimensional motion in a narrow channel around the ring. The potential energy profile felt by the polaritons in the radial direction is approximately harmonic, giving a ladder of quantized states for radial motion separated by about 200 μeV, well below the value of $k_B T$ for the effective temperature of the polaritons, which is about 10 K. (See the Supplemental Material [19] for further details about the radial potential-energy profile). The polariton condensate therefore can have motion in the radial direction.

For these experiments we generated the polaritons by focusing a nonresonant pump laser onto a small spot on one side of the ring. Above the critical density threshold for condensation, the polariton condensate streams ballistically out of the generation region and around the ring, with a momentum which is quite sensitive to the details of the pump spot location and intensity. For a pump spot near the outer edge of the ring, the condensate was injected with momentum moving toward the inner edge, while for a pump spot near the inner edge, the condensate was injected with outward momentum.

We directly viewed the condensate by imaging the light from the condensate coming through the top mirror. This leakage light means that the condensate has radiative decay and therefore must be continuously pumped to have a stable state, but it also provides us with a direct probe of the behavior of the condensate. Figures 1(b)–1(d) show several examples of different patterns in a ring, created by changing the pump location. As seen in these images, the ballistic path of the polaritons wiggles from side to side as it travels around the ring rather than in a perfect circular trajectory. The side-to-side motion of the wiggles is affected both by the kinetic energy of the polaritons and the spin-orbit effect, which gives a term completely analogous to the zitterbewegung effect [16,17]. As shown in Figs. S7, S8, and S9 of the Supplemental Material [19], the spin-orbit effect is necessary to get good fits of the data; if we leave this term out, the frequency of the wiggles changes substantially.

The exact distance traversed by each wiggle in the ring depends both on the kinetic energy of the ballistic motion and on the spin-orbit term discussed below, which gives a "zitterbewegung" effect. Figure 2 shows both experimental and theoretical images of the polariton condensate motion, showing the total intensity as well as the Stokes polarization components. The theoretical model, discussed below, gives good qualitative agreement with the polarization precession around the ring. The side-to-side "wiggles" of the condensate are the result of two effects: the constraint of the
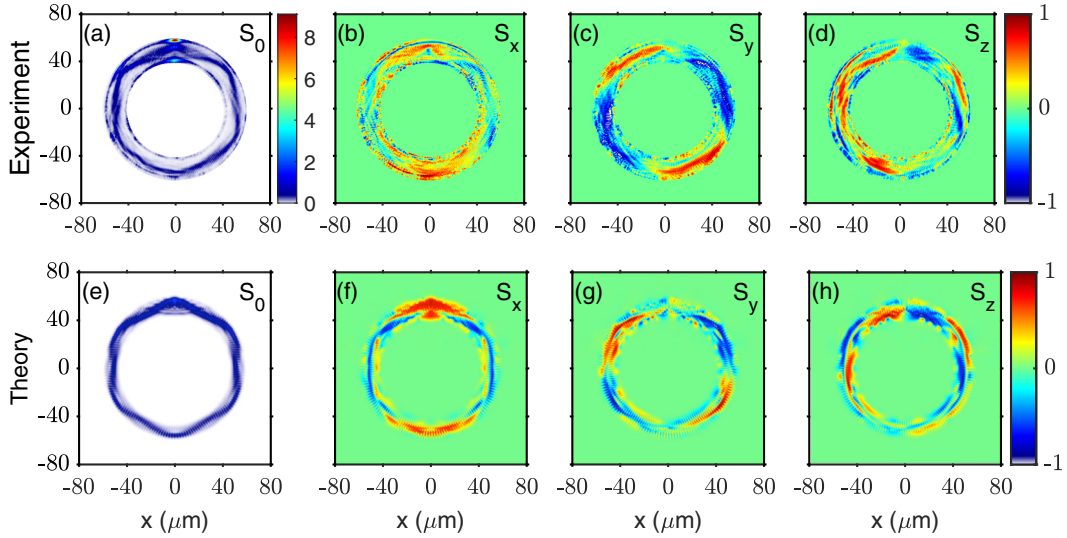
FIG. 2. (a) Experimental data of the polariton condensate with a pump power of $6.1P_{\mathrm{th}}$. The polarization of the pump is 72°. (b)–(d) The three Stokes polarization components. (e)–(h) Theoretical simulation of the condensate and its Stokes components for similar conditions.

quasi-one-dimensional channel of the polaritons and the zitterbewegung effect due to the effective spin-orbit interaction. The Supplemental Material [19] for this paper shows that when the zitterbewegung effect is left out of the theory, the side-to-side motion is substantially affected, to the point that the number of wiggles around the ring is changed.

Figure 3 shows a series of experimental images with the corresponding images generated by the theoretical model for the motion around a ring as the intensity of the pump is increased. The other experimental conditions remained the same. As seen in this figure, the side-to-side motion is washed out at high density.

The polarization of the excitation pump is different for each picture and is recorded in the caption. This is because the pump was at different azimuthal positions of the ring, and we rotated the image so that the pump spot is always at the top. However, the polarization of the pump did not affect the intensity distribution or Stokes vectors of the condensate, as expected since the nonresonant laser excitation creates hot carriers that must emit many phonons before they turn into polaritons (please see the Additional Data of the Experiment section in the Supplemental Material [19]).

III. THEORETICAL ANALYSIS

Our theoretical model is based on prior successful work in modeling coherent polariton condensates with generation and decay [27–31]. In the linear conservative limit, polaritons in the considered system obey the Hamiltonian

$$\hat{H}_0 = \frac{\hbar^2 \hat{k}^2}{2m^*} \hat{\sigma}_0 + V_{\mathrm{st}}(\mathbf{r})\hat{\sigma}_0 + \hbar\hat{\boldsymbol{\Omega}} \cdot \hat{\mathbf{S}}, \tag{1}$$
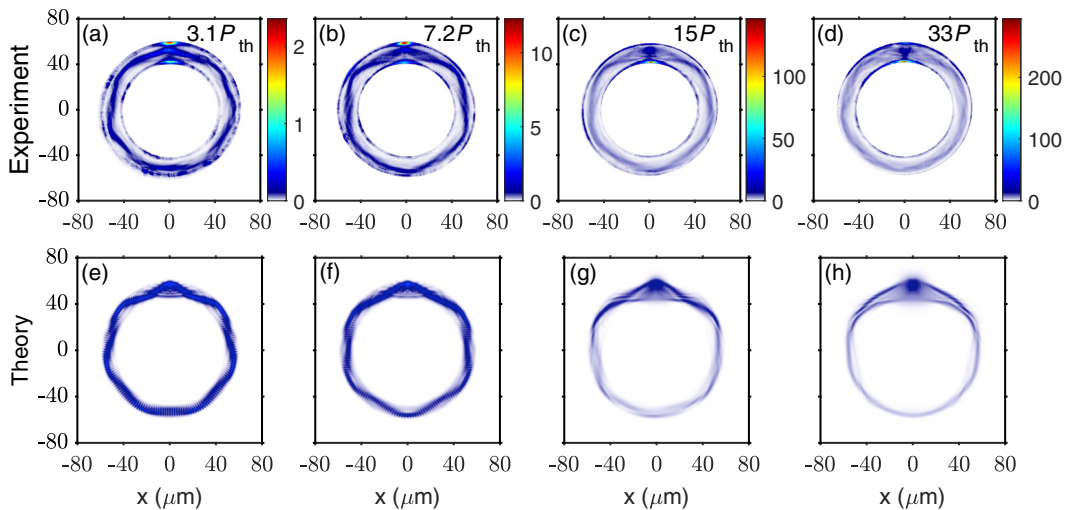

FIG. 3. (a)–(d) A series of experimental condensate images as the pump power was increased from $3.3P_{\mathrm{th}}$ to $32P_{\mathrm{th}}$. The polarization of the pump for panels (a)–(d) is 119°, 72°, 111°, and 108°, respectively. (e)–(h) The corresponding theoretical simulations. Both experimental data and theoretical simulation show that the polygonal PL did not change much with low pump power, but "washed out" at high pump power.
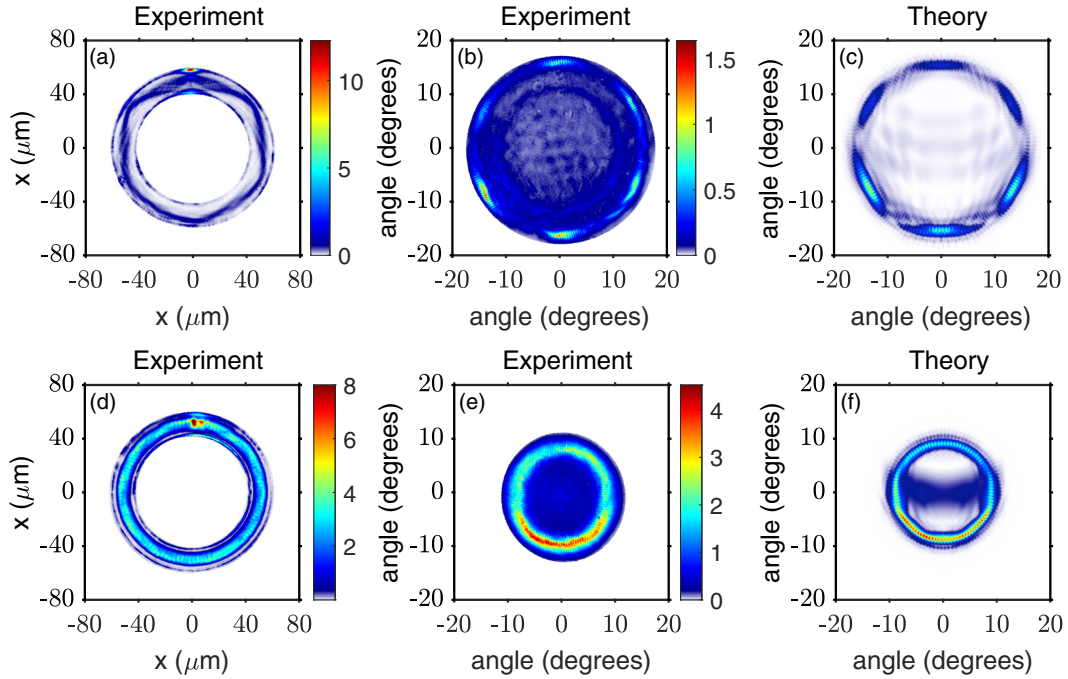
FIG. 4. (a) and (d): Real-space images showing two different patterns due to different radial pumping positions. The pump power was slightly different, $6.1P_{th}$ for panel (a) and $5.3P_{th}$ for panel (d). (b) and (e): The corresponding experimentally measured momentum-space images of panels (a) and (d). (c) and (f): Theoretical momentum-space images for panels (b) and (e).

where m^* is the effective mass of polaritons, and $\hat{\mathbf{k}} = (\hat{k}_x, \hat{k}_y) = (-i\partial_x, -i\partial_y)$ is the quasimomentum operator. $V_{st}(\mathbf{r})$ describes the ring-shaped stationary potential. The Hamiltonian acts on the polariton quantum state described by the spinor $|\Psi\rangle = [\Psi_+(\mathbf{r}), \Psi_-(\mathbf{r})]^T$, where $\Psi_\pm(\mathbf{r})$ are the wave functions of the spin-up and spin-down states. The last term in Eq. (1) is responsible for the spin-orbit interaction (SOI) of polaritons originated from the splitting in the TE- and TM-polarized polariton modes in the layered microcavity structure [31,32]. The effect of SOI can be described as precession of the polariton pseudospin vector $\hat{\mathbf{S}} = (\hat{S}_x, \hat{S}_y, \hat{S}_z)$ around the effective magnetic field $\hat{\mathbf{\Omega}}$ induced by the splitting:

$$\hat{\mathbf{\Omega}} = \left[\Delta(\hat{k}_x^2 - \hat{k}_y^2), 2\Delta\hat{k}_x\hat{k}_y, 0\right], \quad (2)$$

where Δ is the TE-TM splitting constant. The pseudospin vector is introduced as $\hat{\mathbf{S}} = \frac{1}{2}\hat{\boldsymbol{\sigma}}$, where $\hat{\boldsymbol{\sigma}}$ is the vector of the Pauli matrices, and $\hat{\sigma}_0$ is the 2×2 identity matrix.

The trajectory of a ballistically propagating particle is described by the equation of motion for the position operator: $\hbar d_t \hat{r}_j = i[\hat{H}_0, \hat{r}_j]$, where $\hat{r}_j = \hat{x}$ and $\hat{y}$.

The structure considered here supports TE-TM splitting, which significantly modifies the waveguide modes. The SOI component of the Hamiltonian (1) introduces an oscillating term to the equation of motion of the position operator $\hat{\mathbf{r}}$, which is supplemented with the equation of precession of the polariton pseudospin $d_t\hat{\mathbf{S}} = \hat{\mathbf{\Omega}} \times \hat{\mathbf{S}}$.

To underpin the discussed experimental observations, we performed numerical simulations of the behavior of the spinor exciton-polariton condensate in a ring waveguide trap. We use the generalized Pauli equation for the spinor $|\Psi\rangle = [\Psi_+(t, \mathbf{r}), \Psi_-(t, \mathbf{r})]^T$, where $\Psi_\pm(t, \mathbf{r})$ are the wave functions of the spin-up and spin-down states. See details of the model

in the Supplemental Material [19] (see also Refs. [33,34]). To get closer to the experimental conditions, we take into account the effects of interaction of particles and the nonconservative processes of the pump that generates the polaritons and radiative losses.

Polaritons in the system possess a finite lifetime due to escaping photons from the structure through the top mirrors and due to additional damping induced by etching of the microcavity. The latter includes tunneling of photons through the side walls of the ring trap and scattering of polaritons from the rough surface of the walls. This effect can be taken into account by assuming the stationary potential $V_{st}(\mathbf{r})$ to be complex [29,30]. The nonresonant optical pump excites the spinor reservoir of incoherent excitons (in fact, excitonlike polaritons), which plays two important roles in the formation of the polariton intensity patterns. First, it feeds the polariton condensate via stimulated relaxation of particles from it. Second, it contributes to the effective potential landscape for polaritons due to the repulsive interaction of particles in the condensate and the reservoir. The cloud of excitons forms the local potential maximum under the pump spot, the height of which increases with increasing the pump power. Polaritons emerging within the pump spot propagate away from the potential maximum; as they leave, their potential energy is converted to the kinetic energy of ballistic motion. As one can see from Eq. (2), the Larmor frequency of the effective magnetic field depends quadratically on the polariton wave vector. The pump power and the displacement of the pump spot play the role of the control parameters in our system. The density dependence shown in Fig. 3 is modeled simply by turning up the pump power, which increases the role of the nonlinear polariton-polariton and polariton-exciton terms.

Finally, Fig. 4 shows the momentum-space images for both the experimental data (done by recording the Fourier plane of the polariton light emission) and the theory (done by taking the Fourier transform of the solutions of the theoretical model). For purely circular motion in the ring, the k-space distribution will also be a ring. Because the orbitals have favored angles, the k-space distribution is seen as bright spots at specific directions.

IV. CONCLUSIONS

In these experiments, we have shown that we can create stable orbital-like patterns by varying the position of the injection spot, which in turn controls the ballistic injection momentum of the polariton condensate. Our polarization resolution shows that the effective spin-orbit coupling plays a major role in controlling the precession of the polarization around the ring, as well as the effective length of the path for the phase advance. Further, the theoretical analysis shows that the zitterbewegung effect due to the effective spin-orbit coupling plays a substantial role in the orbital pattern of the ballistic condensate.

Bose condensation is crucial for this effect to be seen, because the condensation locks the particles into monoenergetic states with a single ballistic behavior. Without this, the particles would occupy a continuum of modes that would obscure each other in time-integrated imaging.

[1] N. Murray, M. Krygier, M. Edwards, K. C. Wright, G. K. Campbell, and C. W. Clark, Phys. Rev. A **88**, 053615 (2013).

[2] S. Eckel, F. Jendrzejewski, A. Kumar, C. J. Lobb, and G. K. Campbell, Phys. Rev. X **4**, 031052 (2014).

[3] A. Kumar, N. Anderson, W. D. Phillips, S. Eckel, G. K. Campbell, and S. Stringari, New J. Phys. **18**, 025001 (2016).

[4] M. de Goër de Herve, Y. Guo, C. De Rossi, A. Kumar, T. Badr, R. Dubessy, L. Longchambon, and H. Perrin, J. Phys. B: At., Mol. Opt. Phys. **54**, 125302 (2021).

[5] G.-Q. Liu, D. W. Snoke, A. J. Daley, L. N. Pfeiffer, and K. West, Proc. Natl. Acad. Sci. U.S.A. **112**, 2676 (2015).

[6] J. Wang, H. Xu, R. Su, Y. Peng, J. Wu, T. C. H. Liew, and Q. Xiong, Light Sci. Appl. **10**, 45 (2021).

[7] F. Manni, K. G. Lagoudakis, T. C. H. Liew, R. André, and B. Deveaud-Plédran, Phys. Rev. Lett. **107**, 106401 (2011).

[8] A. Dreismann, P. Cristofolini, R. Balili, G. Christmann, F. Pinsker, N. G. Berloff, Z. Hatzopoulos, P. G. Savvidis, and J. J. Baumberg, Proc. Natl. Acad. Sci. U.S.A. **111**, 8770 (2014).

[9] V. K. Kalevich, M. M. Afanasiev, V. A. Lukoshkin, D. D. Solnyshkov, G. Malpuech, K. V. Kavokin, S. I. Tsintzos, Z. Hatzopoulos, P. G. Savvidis, and A. V. Kavokin, Phys. Rev. B **91**, 045305 (2015).

[10] V. A. Lukoshkin, V. K. Kalevich, M. M. Afanasiev, K. V. Kavokin, Z. Hatzopoulos, P. G. Savvidis, E. S. Sedov, and A. V. Kavokin, Phys. Rev. B **97**, 195149 (2018).

[11] Y. Sun, Y. Yoon, S. Khan, L. Ge, M. Steger, L. N. Pfeiffer, K. West, H. E. Türeci, D. W. Snoke, and K. A. Nelson, Phys. Rev. B **97**, 045303 (2018).

[12] E. Schrodinger, Sitzungsber. Preuss. Akad. Wiss., Phys.-Math Kl. **24**, 418 (1930).

[13] R. Gerritsma, G. Kirchmair, F. Zahringer, E. Solano, R. Blatt, and C. F. Roos, Nature (London) **463**, 68 (2010).

[14] J. Schliemann, D. Loss, and R. M. Westervelt, Phys. Rev. B **73**, 085323 (2006).

[15] L. J. LeBlanc, M. C. Beeler, K Jiménez-García, A. R. Perry, S. Sugawa, R. A. Williams, and I. B. Spielman, New J. Phys. **15**, 073011 (2013).

[16] E. S. Sedov, Y. G. Rubo, and A. V. Kavokin, Phys. Rev. B **97**, 245312 (2018).

[17] E. S. Sedov, I. E. Sedova, S. M. Arakelian, and A. V. Kavokin, Opt. Lett. **46**, 1836 (2021).

[18] S. Mukherjee, V. K. Kozin, A. V. Nalitov, I. A. Shelykh, Z. Sun, D. M. Myers, B. Ozden, J. Beaumariage, M. Steger, L. N. Pfeiffer, K. West, and D. W. Snoke, Phys. Rev. B **103**, 165306 (2021).

[19] See Supplemental Material at http://link.aps.org/supplemental/10.1103/PhysRevB.106.245309 for more details about the experiment and the numerical model.

[20] J. Kasprzak, M. Richard, S. Kundermann, A. Baas, P. Jeanbrun, J. M. J. Keeling, R. Andre, J. L. Staehli, V. Savona, P. B. Littlewood, B. Deveaud, and L. S. Dang, Nature (London) **443**, 409 (2006).

[21] R. Balili, V. Hartwell, D. W. Snoke, L. Pfeiffer, and K. West, Science **316**, 1007 (2007).

[22] P. Littlewood and A. Edelman, in *Universal Themes of Bose-Einstein Condensation*, edited by N. Proukakis, D. W. Snoke, and P. B. Littlewood (Cambridge University, Cambridge, England, 2017).

[23] Y. Sun, P. Wen, Y. Yoon, G.-Q. Liu, M. Steger, L. N. Pfeiffer, K. West, D. W. Snoke, and K. A. Nelson, Phys. Rev. Lett. **118**, 016602 (2017); **118**, 149901 (2017).

[24] M. Steger, G.-Q. Liu, B. Nelsen, C. Gautham, D. W. Snoke, R. Balili, L. N. Pfeiffer, and K. West, Phys. Rev. B **88**, 235314 (2013).

[25] M. Steger, C. Gautham, D. W. Snoke, L. N. Pfeiffer, and K. West, Optica **2**, 1 (2015).

[26] S. Mukherjee, D. M. Myers, R. G. Lena, B. Ozden, J. Beaumariage, Z. Sun, M. Steger, L. N. Pfeiffer, K. West, A. J. Daley, and D. W. Snoke, Phys. Rev. B **100**, 245304 (2019).

[27] I. I. Ryzhov, V. O. Kozlov, N. S. Kuznetsov, I. Yu. Chestnov, A. V. Kavokin, A. Tzimis, Z. Hatzopoulos, P. G. Savvidis, G. G. Kozlov, and V. S. Zapasskii, Phys. Rev. Res. **2**, 022064(R) (2020).

[28] E. S. Sedov, I. E. Sedova, S. M. Arakelian, and A. V. Kavokin, New J. Phys. **22**, 083059 (2020).

[29] J. Beierlein, E. Rozas, O. A. Egorov, M. Klaas, A. Yulin, H. Suchomel, T. H. Harder, M. Emmerling, M. D. Martín, I. A. Shelykh, C. Schneider, U. Peschel, L. Viña, S. Höfling, and S. Klembt, Phys. Rev. Lett. **126**, 075302 (2021).

[30] I. Sedova and E. Sedov, Results Opt. **4**, 100105 (2021).

[31] G. Panzarini, L. C. Andreani, A. Armitage, D. Baxter, M. S. Skolnick, V. N. Astratov, J. S. Roberts, Alexey V. Kavokin, Maria R. Vladimirova, and M. A. Kaliteevski, Phys. Rev. B **59**, 5082 (1999).

[32] G. Panzarini, L. C. Andreani, A. Armitage, D. Baxter, M. S. Skolnick, V. N. Astratov, J. S. Roberts, A. V. Kavokin, M. R. Vladimirova, and M. A. Kaliteevski, Phys. Solid State **41**, 1223 (1999).

[33] A. Kavokin, J. Baumberg, G. Malpuech, and F. Laussy, *Microcavities*, 2nd ed., Series on Semiconductor Science and Technology (Oxford University, Oxford, 2017).

[34] M. Z. Maialle, E. A. de Andrada e Silva, and L. J. Sham, Phys. Rev. B **47**, 15776 (1993).